Membrane and Water Treatment, *Vol. 17, No. 2 (2026) 103-119*
https://doi.org/10.12989/mwt.2026.17.2.103

Hydrodynamic performance of nanocomposite structures in sports water systems: enhancing efficiency in athletic hydration

Kun Li[1], A. Horri[2], F. Ming*[3]

[1]*Sports Institute., Henan University of Technology, Henan Province, 450000, China*
[2]*Department of Civil Engineering, University of Zabol, Zabol, Iran*
[3]*Department of Engineering, Malaya University, Malaysia*

(Received March 13, 2024, Revised September 9, 2025, Accepted December 30, 2025)

Abstract. The hydrodynamic performance optimization of sports water systems is a mandatory consideration to improve the efficiency in sports hydration. In the given research, the concept of nanocomposites structures is proposed as a method of improving fluid delivery and structural integrity of high-performance hydration pipelines in the context of competitive sports environments. We also discuss the application of nano-engineered concrete pipelines created in the research and development of nano-conduits in polymers as portable and submersible sports hydration to inspired by the advances in nano-engineered concrete pipelines to pump fluids on a mass scale. The governing equations of motion are developed using classical shell theory and Hamilton principle and the fluid-structure interactions are modeled according to the framework of Navier Stokes equations. The successful material properties of the nanocomposites are estimated with the assistance of the Mori-Tanaka method. They are determined by taking dynamic simulations, which are based on the numerical techniques such as the differential quadrature method (DQM) and the Newmark method, to the system in response to various loads, such as fluid pressure changes and external dynamic disturbances. Results show nanoparticle reinforcement compound to increase rigidity, reduce peak deflections and augmenting resistance to vibrational instabilities, however the mass of internal fluids has an overwhelming influence on modal behaviors. The parametric studies indicate that the hydrodynamic efficiency is highly dependent on geometrical ratios (thickness/ radius, length/ radius) and boundary conditions and volumes fractions of nanoparticles. The findings indicate that optimized nanocomposite pipelines are applicable to minimize the energy losses incurred in the transportation of fluids, as well as provide structural stability in the dynamic application by athletes in next-generation athletic sports hydration technologies.

Keywords: athletic hydration efficiency; fluid-structure interaction; hydrodynamic performance; nano-composite structures; sports water systems

1. Introduction

Effective hydration is an essential need in the sports performance that directly affects the endurance, athletes' recovery, and physiological stability. Contemporary sports water systems are specified to achieve the maximum delivery and transference, but many classical structures of fluid transfer are commonly constrained in aspects of longevity, hydrodynamic effectiveness, and activity against external interferences. The recent developments in nanotechnology and composite

*Corresponding author, Ph.D., E-mail: f.ming.must@gmail.com

ISSN: 2005-8624 (Print), 2092-7037 (Online)

materials present the opportunities to work around those issues by improving both the structural and fluid-dynamic characteristics of hydration conduits. Nanoparticles like SiO_2 have been extensively investigated to enhance mechanical and functional performance of large-scale pipeline systems especially during dynamic environments like earthquake loading and varying internal pressure. Application of these principles to the sports water system gives a special guide to the creation of lightweight, robust, and efficient hydration system and the system that would survive in complex conditions of operation, such as vibrations caused by motion and changes in flow demands.

Fluid-structure interaction of shell-like structures The fluid-structure interaction problem has been treated with unparalleled importance due to its intrinsic interest in engineering, energy transport and structural interactions. The earliest literature [1] started with the dynamics of the articulated pipes that carried fluid and then the study later advanced to the nonlinear vibration and stability analysis of the cylindrical shells and pipes that had internal flow [2, 3]. The other analysis was an analysis by Amabili [4] which was a model of nonlinear vibrations and stability of shells and plates and which have been employed to give the basis of modeling of the fluid-conveying structures when subjected to dynamic loading. The past few years have seen the significant development of studying the complex mechanisms of nonlinear resonances, vibrational instability, and composite and nanocomposite pipelines buckling [5-8]. The advanced numerical solution of multi-span pipeline and composite shells like wavelet-based finite elements and dynamic softness-based methods has been utilized [9-10]. The cracks have also been generalized in their contribution to the stability of fluid carrying pipes, as well as distributed forces and elastic supports in their contribution to non-linear dynamics of pipes [11-12]. Besides structural developments, in water transportation, as in water distribution systems, has also become a major concern in its application under seismic and environmental hazards. One such source is Youn et al. [13], which had established the priority structures of pipeline renewal under the conditions of seismic susceptibility, and Zamani Nouri [14] had modeled CNT-reinforced concrete pipes to enhance the stability of vibration. It has also been shown that nanomaterials can also increase rigidity, dynamic response and energy efficiency in fluid-carrying conduits when incorporated. Remarkably, [15] also indicated the opportunities of employing nanoparticles in the quest to enhance quality of water by utilizing them to hydrate sport related systems and consequently connect the science of material science to the application sector, i.e. sports. Other perspectives, such as the use of fluid dynamics to art-inspired approaches also observe that the flow structure analysis can be applied to a broad range of other disciplines [16]. It is based on these reasons that the present study explores the hydrodynamic behaviour of nanocomposites pipelines in sport water systems with particular consideration on how optimization of efficiency can be achieved in sport hydration. The difference between sport hydrating pipelines and the conventional bulk fluid transport systems is that a high-speed fluid transport system should be light, strong and energy-efficient to resist exterior disturbance and vibration that accompanies motion in relation to the conventional large-scale fluid transport systems. The current analysis employs the classical shell theory, Hamilton principal theory, fluid structure interaction theory based on the Navier Stokes equations when attempting to determine the effects of nanoparticle reinforcement on the vibration response, the stability and flow efficiency. The Mori-Tanaka technique helps to determine the effective material properties of nanocomposites, and numerical calculation is performed with the help of the differential quadrature method (DQM) and the Newmark scheme.

This paper evaluates the hydrodynamic behavior of nanocomposite pipelines as a sports hydration system, which considers fluid-structure interaction modeling and the contribution of

nanoparticle reinforcing agents. Classical shell theory and Hamilton principle are used to derive governing equations and the internal and external fluid dynamics are approximated by the Navier-Stokes equations. MoriTanaka method is used in estimating the equivalent behavior of nano-composite material and the computing of the numerical simulation is performed with the help of the differential quadrature method (DQM) and Newmark integration scheme. An elaborate parametric study is performed to examine the effects of nanoparticle concentration, geometrical ratios, boundary conditions and internal fluid pressure on system response.

This work of study is novel in that it brings nanocomposite structural design, which has been used in large-scale energy pipelines, into the new area of application in sports water systems used in athletic hydration. This study proposes a hydronic-structural optimization process in contrast to the available hydration technologies that focus more on ergonomics and portability, and provides a direct connection between material engineering and fluid efficiency. The proposed system, which incorporates the reinforcing structure of SiO_2 nanoparticle into the polymer-based hydration conduits, exhibits better rigidity, lesser vibrational deflection and greater hydrodynamic flow stability when the system is subjected to conditions of dynamic loading. The framework is an interdisciplinary approach spanning between sports engineering, nanomaterials and fluid mechanics that offers a new avenue in designing high-performance hydration systems that are lightweight, durable, as well as energy-efficient.

2. Mathematical modeling

The system that is being studied, as shown in Fig. 1, is a pipeline that is an underwater nanocomposite cylindrical pipe that contains internal fluid. The structure of the pipe is represented by a length a, radius R and wall thickness h where the pipeline is a thin walled cylindrical shell structure that interacts with the inside fluid environment and external fluid environment. To achieve the baseline configuration, the support conditions at the two ends of the pipe are taken to be simply supported, so that it is realistic, allowing both flexibility and displacement response, and further comparison with other support conditions in subsequent parametric studies. SiO_2 (silica) nanoparticles that are uniformly dispersed in the polymeric matrix are added to the pipe material to increase the mechanical and hydrodynamic characteristics of the structure. The default volume fraction of the nanoparticles is 0.05, which is a typical reinforcement level studied, and in which the particle volume fraction can be increased significantly to obtain high stiffness and vibration damping without causing aggregation effects or excessive density increases.

The classic theory is:

$$u_1(x,\theta,z,t) = u(x,\theta,t) - z\frac{\partial w(x,\theta,t)}{\partial x}, \tag{1}$$

$$u_2(x,\theta,z,t) = v(x,\theta,t) - \frac{z}{R}\frac{\partial w(x,\theta,t)}{\partial \theta}, \tag{2}$$

$$u_3(x,\theta,z,t) = w(x,\theta,t), \tag{3}$$

where (u_1, u_2, u_3) denotes the displacement components at an arbitrary point (x, θ, z) in the shell, and (u, v, w) are the displacement components of the middle surface of the shell in the axial, circumferential and radial directions, respectively. The strain-displacement relationships are:

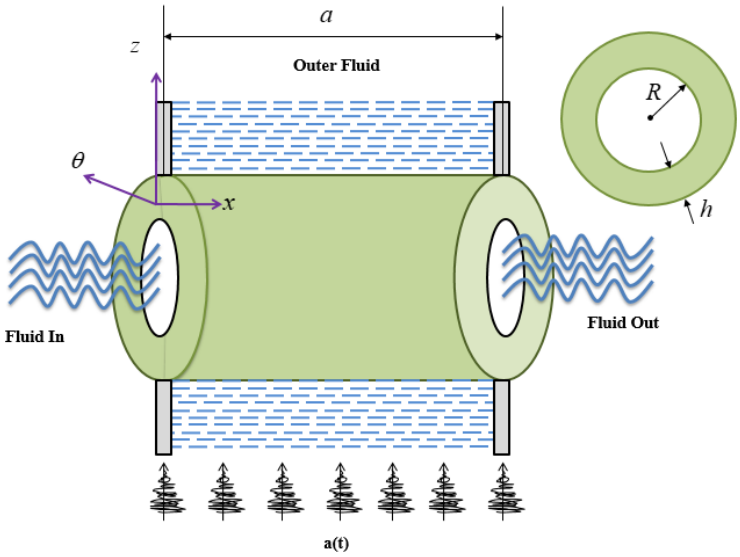

Figure 1. Schematic of underwater concrete pipe conveying fluid under earthquake load

$$\varepsilon_{xx} = \frac{\partial u}{\partial x} - z\frac{\partial^2 w}{\partial x^2}, \tag{4}$$

$$\varepsilon_{\theta\theta} = \frac{\partial v}{R\partial\theta} + \frac{w}{R} - \frac{z}{R^2}\frac{\partial^2 w}{\partial\theta^2}, \tag{5}$$

$$\varepsilon_{xy} = \frac{1}{2}\left(\frac{\partial u}{R\partial\theta} + \frac{\partial v}{\partial x}\right) - z\frac{\partial^2 w}{R\partial x\partial\theta}, \tag{6}$$

where $(\varepsilon_{xx}, \varepsilon_{\theta\theta})$are the normal strain components and $(\varepsilon_{x\theta})$ is the shear strain component. The stress relations are:

$$\begin{bmatrix}\sigma_{xx}\\ \sigma_{\theta\theta}\\ \tau_{x\theta}\end{bmatrix} = \begin{bmatrix}C_{11} & C_{12} & 0\\ C_{21} & C_{22} & 0\\ 0 & 0 & C_{66}\end{bmatrix}\begin{bmatrix}\varepsilon_{xx}\\ \varepsilon_{\theta\theta}\\ \gamma_{x\theta}\end{bmatrix}, \tag{7}$$

Based on Mori and Tanaka method for the effect of nanoparticles, we have:

$$\begin{Bmatrix}\sigma_{xx}\\ \sigma_{yy}\\ \sigma_{zz}\\ \sigma_{yz}\\ \sigma_{xz}\\ \sigma_{xy}\end{Bmatrix} = \begin{bmatrix}\underbrace{k+m}_{C_{11}} & \underbrace{l}_{C_{12}} & \underbrace{k-m}_{C_{13}} & 0 & 0 & 0\\ \underbrace{l}_{C_{21}} & \underbrace{n}_{C_{22}} & \underbrace{l}_{C_{23}} & 0 & 0 & 0\\ \underbrace{k-m}_{C_{31}} & \underbrace{l}_{C_{32}} & \underbrace{k+m}_{C_{33}} & 0 & 0 & 0\\ 0 & 0 & 0 & \underbrace{p}_{C_{44}} & 0 & 0\\ 0 & 0 & 0 & 0 & \underbrace{m}_{C_{55}} & 0\\ 0 & 0 & 0 & 0 & 0 & \underbrace{p}_{C_{66}}\end{bmatrix}\begin{Bmatrix}\varepsilon_{xx}\\ \varepsilon_{yy}\\ \varepsilon_{zz}\\ \gamma_{yz}\\ \gamma_{xz}\\ \gamma_{xy}\end{Bmatrix}, \tag{8}$$

where $\sigma_{ij}, \varepsilon_{ij}, \gamma_{ij}, k, m, n, l, p$ are the stress components, the strain components and the stiffness coefficients, respectively. According to the Mori-Tanaka method, the stiffness coefficients are given by:

$$\begin{aligned}
k &= \frac{E_m\{E_m c_m + 2k_r(1+\nu_m)[1+c_r(1-2\nu_m)]\}}{2(1+\nu_m)[E_m(1+c_r-2\nu_m)+2c_m k_r(1-\nu_m-2\nu_m^2)]} \\
l &= \frac{E_m\{c_m\nu_m[E_m+2k_r(1+\nu_m)]+2c_r l_r(1-\nu_m^2)]\}}{(1+\nu_m)[E_m(1+c_r-2\nu_m)+2c_m k_r(1-\nu_m-2\nu_m^2)]} \\
n &= \frac{E_m^2 c_m(1+c_r-c_m\nu_m)+2c_m c_r(k_r n_r - l_r^2)(1+\nu_m)^2(1-2\nu_m)}{(1+\nu_m)[E_m(1+c_r-2\nu_m)+2c_m k_r(1-\nu_m-2\nu_m^2)]} \\
&\quad + \frac{E_m[2c_m^2 k_r(1-\nu_m)+c_r n_r(1+c_r-2\nu_m)-4c_m l_r\nu_m]}{E_m(1+c_r-2\nu_m)+2c_m k_r(1-\nu_m-2\nu_m^2)} \\
p &= \frac{E_m[E_m c_m + 2p_r(1+\nu_m)(1+c_r)]}{2(1+\nu_m)[E_m(1+c_r)+2c_m p_r(1+\nu_m)]} \\
m &= \frac{E_m[E_m c_m + 2m_r(1+\nu_m)(3+c_r-4\nu_m)]}{2(1+\nu_m)\{E_m[c_m+4c_r(1-\nu_m)]+2c_m m_r(3-\nu_m-4\nu_m^2)\}}
\end{aligned} \tag{9}$$

where C_m and C_r are the volume fractions of the concrete and the SiO_2 nano-particles, respectively. Also k_r, l_r, n_r, p_r, m_r are the Hills elastic modulus.

3. Motion equations

The potential energy is:

$$U = \int_V (\sigma_{xx}\varepsilon_{xx} + \sigma_{\theta\theta}\varepsilon_{\theta\theta} + \sigma_{x\theta}\gamma_{x\theta})\, dV, \tag{10}$$

By substituting Eqs. (4)-(6) into (10) yields:

$$\begin{aligned}
U = \int_{-\frac{h}{2}}^{\frac{h}{2}} \int_A \Bigg(& \sigma_x \left(\frac{\partial u}{\partial x} - z\frac{\partial^2 w}{\partial x^2} \right) + \sigma_\theta \left(\frac{\partial v}{R\partial\theta} + \frac{w}{R} - z\frac{\partial^2 w}{R^2\,\partial\theta^2} \right) \\
& + \sigma_{x\theta} \left(\frac{\partial u}{R\partial\theta} + \frac{\partial v}{\partial x} - 2z\frac{\partial^2 w}{R\partial\theta\partial x} \right) \Bigg) dz dA
\end{aligned} \tag{11}$$

By introducing force and moment as:

$$\begin{Bmatrix} N_x \\ N_\theta \\ N_{x\theta} \end{Bmatrix} = \int_{-\frac{h}{2}}^{\frac{h}{2}} \begin{Bmatrix} \sigma_x \\ \sigma_\theta \\ \tau_{x\theta} \end{Bmatrix} dz, \tag{12}$$

$$\begin{Bmatrix} M_x \\ M_\theta \\ M_{x\theta} \end{Bmatrix} = \int_{-\frac{h}{2}}^{\frac{h}{2}} \begin{Bmatrix} \sigma_x \\ \sigma_\theta \\ \tau_{x\theta} \end{Bmatrix} z dz, \tag{13}$$

$$U = \int_A \left(N_x \left(\frac{\partial u}{\partial x} \right) - M_x \frac{\partial^2 w}{\partial x^2} + N_\theta \left(\frac{\partial v}{R\partial\theta} + \frac{w}{R} \right) - M_\theta \frac{\partial^2 w}{R^2\,\partial\theta^2} - 2M_{x\theta} \frac{\partial^2 w}{R\partial\theta\partial x} + N_{x\theta} \left(\frac{\partial u}{R\partial\theta} + \frac{\partial v}{\partial x} \right) \right) dA \tag{14}$$

The kinetic energy is:

$$K = \frac{\rho}{2} \int_v \left((\frac{\partial u_1}{\partial t})^2 + (\frac{\partial u_2}{\partial t})^2 + (\frac{\partial u_3}{\partial t})^2 \right) dV, \tag{15}$$

By substituting Eqs. (1)– (3) into (15) and defining the following term

$$\begin{Bmatrix} h \\ 0 \\ \frac{h^3}{12} \end{Bmatrix} = \int_{-h/2}^{h/2} \begin{bmatrix} 1 \\ z \\ z^2 \end{bmatrix} dz, \tag{16}$$

We have

$$K = \int \left(\frac{\rho}{2} \left(\frac{h^3}{12} \left((\frac{\partial^2 u}{\partial t \partial x})^2 + (\frac{\partial^2 w}{\partial t \partial \theta})^2 \right) \right) + h \left((\frac{\partial u}{\partial t})^2 + (\frac{\partial v}{\partial t})^2 + (\frac{\partial w}{\partial t})^2 \right) \right) dA. \tag{17}$$

The Navier-Stokes equation is:

$$\rho_f \frac{dV}{dt} = -\nabla P + \mu \nabla^2 V + F_{body}, \tag{18}$$

where

$$\frac{d}{dt} = \frac{\partial}{\partial t} + v_x \frac{\partial}{\partial x} + v_\theta \frac{\partial}{\partial \theta} + v_z \frac{\partial}{\partial z}, \tag{19}$$

in which $V = (v_x, v_\theta, v_z)$ is the flow velocity vector in cylindrical coordinate system with components in longitudinal x, circumferentialθ and radial z directions. Also, P and ρ_f are the pressure the density of the fluid, respectively and F_{body} denotes the body forces. At the point of contact between the fluid and the core, the relative velocity and acceleration in the radial direction are equal. So

$$v_z = \frac{dw}{dt}, \tag{20}$$

By employing Eqs. (19, 20) we have:

$$\frac{\partial p_z}{\partial z} = -\rho_f \left(\frac{\partial^2 w}{\partial t^2} + 2\, v_x \frac{\partial^2 w}{\partial x \partial t} + {v_x}^2 \frac{\partial^2 w}{\partial x^2} \right) + \mu \left(\frac{\partial^3 w}{\partial x^2 \partial t} + \frac{\partial^3 w}{R^2 \partial \theta^2 \partial t} + v_x \left(\frac{\partial^3 w}{\partial x^3} + \frac{\partial^3 w}{R^2 \partial \theta^2 \partial x} \right) \right) \tag{21}$$

Also,

$$F_{fluid} = A\frac{\partial p_z}{\partial z} = -\rho_f\left(\frac{\partial^2 w}{\partial t^2} + 2\,v_x\frac{\partial^2 w}{\partial x \partial t} + {v_x}^2\frac{\partial^2 w}{\partial x^2}\right) + \mu\left(\frac{\partial^3 w}{\partial x^2 \partial t} + \frac{\partial^3 w}{R^2 \partial \theta^2 \partial t} + v_x\left(\frac{\partial^3 w}{\partial x^3} + \frac{\partial^3 w}{R^2 \partial \theta^2 \partial x}\right)\right) \tag{22}$$

Finally, the external work is:

$$W_f = \int (F_{fluid}) w dA = \int \left(-\rho_f\left(\frac{\partial^2 w}{\partial t^2} + 2v_x\frac{\partial^2 w}{\partial x \partial t} + {v_x}^2\frac{\partial^2 w}{\partial x^2}\right) + \mu\left(\frac{\partial^3 w}{\partial x^2 \partial t} + \frac{\partial^3 w}{R^2 \partial \theta^2 \partial t} + v_x\left(\frac{\partial^3 w}{\partial x^3} + \frac{\partial^3 w}{R^2 \partial \theta^2 \partial x}\right)\right)\right) w dA, \tag{23}$$

Also, the external work is:

$$F_v = -\alpha\frac{\partial w}{\partial t}, \tag{24}$$

where

$$\alpha = \frac{2\nu_f \pi(\eta^2 - 1)}{(1 - \eta^2 + (\eta^2 + 1)\,ln\,\eta)} \;\; and \eta = \frac{R_0}{R_1} \tag{25}$$

In final, the external force is:

$$q = F_v \tag{26}$$

The external work can be given as:

$$W_s = \int (\underbrace{ma(t)}_{F_{Seismic}}) w dA, \tag{27}$$

where *m* and *a(t)* are the mass and the acceleration of the ground. The Hamilton's principle is:

$$\int_0^t (\delta U - \delta K - \delta W) dt = 0. \tag{28}$$

Now, by applying the Hamilton's principle we have:

$$\frac{\partial N_x}{\partial x} + \frac{\partial N_{x\theta}}{R\partial\theta} = \rho h\frac{\partial^2 u}{\partial t^2}, \tag{29}$$

$$\frac{\partial N_\theta}{R\partial\theta} + \frac{\partial N_{x\theta}}{\partial x} = \rho h\frac{\partial^2 v}{\partial t^2}, \tag{30}$$

$$\frac{\partial^2 M_x}{\partial x^2} + \frac{2\partial^2 M_{x\theta}}{R\partial x\partial\theta} + \frac{\partial^2 M_\theta}{R^2\partial\theta^2} - \frac{N_\theta}{R} + N_x\frac{\partial^2 w}{\partial x^2} + N_\theta\frac{\partial^2 w}{R^2\partial\theta^2} + N_{x\theta}\frac{2\partial^2 w}{R\partial x\partial\theta} + F_V + F_{fluid} = \rho h\frac{\partial^2 w}{\partial t^2} + F_{Seismic}, \tag{31}$$

By integrating the stress-strain relations we have

$$N_x = h\left(C_{11}\left(\frac{\partial u}{\partial x}\right) + C_{12}\left(\frac{\partial v}{R\partial\theta} + \frac{w}{R}\right)\right), \tag{32}$$

$$N_\theta = h\left(C_{12}\left(\frac{\partial u}{\partial x}\right) + C_{22}\left(\frac{\partial v}{R\partial\theta} + \frac{w}{R}\right)\right), \tag{33}$$

$$N_{x\theta} = h\left(C_{66}\left(\frac{\partial u}{R\partial\theta} + \frac{\partial v}{\partial x}\right)\right), \tag{34}$$

$$M_x = \frac{h^3}{12}\left(C_{11}\left(-z\frac{\partial^2 w}{\partial x^2}\right) + C_{12}\left(-z\frac{\partial^2 w}{R^2\,\partial\theta^2}\right)\right) \tag{35}$$

$$M_\theta = \frac{h^3}{12}\left(C_{12}\left(-z\frac{\partial^2 w}{\partial x^2}_x\right) + C_{22}\left(-z\frac{\partial^2 w}{R^2\,\partial\theta^2}\right)\right), \tag{36}$$

$$M_{x\theta} = \frac{h^3}{12}C_{66}\left(-2z\frac{\partial^2 w}{R\partial\theta\partial x}\right). \tag{37}$$

4. Solution

One of the most useful numerical techniques in the solution of complex engineering problems, which involve a combination of structural and fluid interaction, is the Finite Element Method (FEM). Applied to continuing structures, pipelines, cylindrical shells FEM can be utilized to handle continuous structures into small finite elements to obtain the suitable representations of the displacement fields, the position of stress distribution and the nature of vibration under dynamic loading. It is a local deformation capturing method where the pipe is divided into elements with respect to both length and thickness of the pipe, and provides a high fidelity prediction of global responses [17-20].

This would particularly be useful to nanocomposite pipelines, where heterogeneous material behaviour based on the reinforcement of the material with nanoparticles needs to be modeled effectively to determine the impact of stiffness, damping, and mass. In the case of fluid-structure interaction, FEM can be used with governing equations of fluid dynamics to incorporate the effect of internal and external fluids on the structure response. It is usual to combine structural equations with the Navier-Stokes equations of fluid motion, where pressure and velocity fields have been introduced to the equations to allow FEM to compute the interactions of deformation and flow between them. This type of coupled simulation is required in pipelines operating in the underwater environment or sports hydration network where varying flow rates, extraneous behavior and hydrodynamic forces are significant factors in structural performance [21-24].

Moreover, through advanced FEM modeling, one can introduce changes in the boundary conditions, crack propagation and nonlinearities onto materials, which offers an all-inclusive

platform to investigate the reliability of the system when placed within realistic operating environments [25-29]. In addition to this, FEM can provide a strong platform to perform parametric analysis and optimization during the design of the nanocomposite pipeline. The best combinations can be calculated with the use of FEM simulation at the system level by systematically varying the parameters such as nanoparticle volume fraction, thickness to radius ratio, length to radius ratio and boundary supports to minimize deflection, enhance rigidity, and maximize hydrodynamic efficiency. Unlike purely-analytical models, FEM does admit geometric irregularities and complex loading conditions, and thus is fundamental to the translation of theoretical models into reality [30-34].

The FEM is a valuable instrument in optimization of the hydrodynamic performance of sports hydration systems where light weight structures are required in order to weigh up durability and high flow efficiency; structural strengthening and assemblage of the systems are carried out with the FEM. Based on this method, we have:

$$([K]+\Omega[C]+\Omega^2[M])\begin{Bmatrix}\{d_b\}\\ \{d_d\}\end{Bmatrix}=\begin{Bmatrix}\{0\}\\ -Ma(t)\end{Bmatrix}, \tag{38}$$

where K , C ,M , d_b and d_d represent the stiffness matrix, the damping matrix, the mass matrix, the boundary points and domain points, respectively [35-37].

5. Numerical results and discussion

Numerical simulations have been conducted to assess the hydrodynamic behaviour and dynamic behaviour of the nanocomposite cylindrical pipeline to transport fluid under different operating conditions. The base case was a comparison with a simply supported pipe made of a nanoparticle reinforcement volume fraction equal to 0.05. Findings indicate that the addition of SiO_2 nanoparticles can greatly enhance the rigidity of the structure and cause apparent decreases in peak displacement and vibration amplitude under dynamic fluid loading. In addition, it was discovered that the interplay between internal fluid motion and structural deformation is a critical factor that governs the overall stability with fluid mass playing a role towards increasing of effective inertia, and altering the natural frequency of the system. In order to have a systematic investigation on these effects, parametric studies were carried out by changing the conditions of the boundary condition, geometric ratios, nanoparticle concentration, and the internal pressure levels, and the results are discussed and presented in the subsequent subsections.

In the absence of similar publications in the literature covering the same scope of the problem, one cannot directly validate the results found here. Therefore, the present work could be partially validated based on a simplified analysis without considering the nonlinear terms of the governing equations and by comparing the linear dynamic response of the pipe which obtained by DQ and exact methods. Considering the material properties, the same as those reported in first paragraph of section 4, it can be concluded that DQM method is accurate and acceptable for present problem because the present results closely match with the analytical method illustrated in Fig. 2.

The convergence and accuracy of DQ method in evaluating the maximum deflection of the underwater pipe conveying fluid with CC boundary condition is illustrated in Table 1. The results are offered for different values of the DQM grid points. It is found that 15 DQ grid points can yield accurate results. So, the results presented below are based on the number of grid points 15 for DQ solution method.

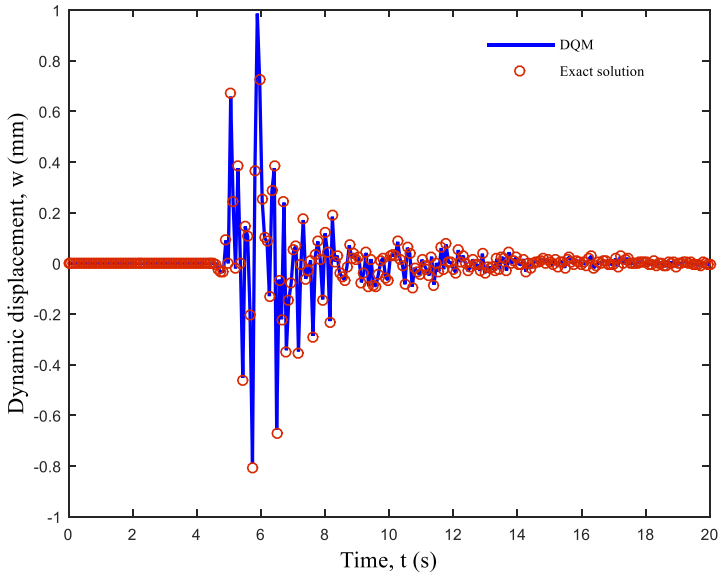

Figure 2. Comparison of the present work with the Exact solution

Table 1. The convergence and accuracy of DQM

DQM points	Max. dynamic deflection
5	4.1089 mm
7	3.9421 mm
9	1.9717 mm
11	1.1832 mm
13	1.0881 mm
15	1.0856 mm
16	1.0855 mm
17	1.0855 mm
18	1.0855 mm

Table 2. Comparison of maximum dynamic deflection with and without internal/external fluid

Condition	Maximum Dynamic Deflection (mm)	Relative Change
Empty pipe (no internal fluid)	0.2	–
Pipe with internal fluid	1.0	+400%
Pipe without external fluid	0.35	–
Pipe with external fluid	1.0	+185%

Table 2 offers a direct quantitative comparison of the highest dynamic deflections of pipelines when the fluid varies. As can be seen, the structural response is dramatically enhanced with the addition of internal fluid; the minimum deflection is almost five times greater than when the pipeline is empty. This large increase can be explained by the added mass effect and decreased

Table 3 The effect of thickness to radius ratio on the maximum dynamic deflection

h/R	Max. dynamic deflection
0.01	1.7407 mm
0.02	1.5122 mm
0.03	1.2412 mm
0.04	0.9856 mm
0.05	0.9221 mm
0.06	0.8811 mm
0.07	0.8656 mm
0.08	0.8412 mm
0.09	0.8309 mm

Table 4. The effect of length to radius ratio on the maximum dynamic deflection

a/R	Max. dynamic deflection
5	1.0831 mm
7	1.1223 mm
10	1.3856 mm
12	1.5529 mm
15	1.8108 mm
17	2.3317 mm
20	2.7941 mm
30	2.8277 mm
0.09	0.8309 mm

rigidity due to the effects of fluid-structure interaction within the pipe. External fluid on the other hand also exhibits a significant destabilizing effect: the lack of outside flow leads to a comparatively lower deflection, whereas the addition of the surrounding fluid leads to a maximum displacement that is increased by about 185%. The mechanical effect of this is that the outer fluid provides hydrodynamic mass and decreases effective rigidity of the system, decreasing the natural frequency and increasing the pipeline to seismic excitation.

Table 3 show the effect of the ratio thickness-to-radius of the pipeline on its dynamic deflection with time. The performance is indicated in a clear way, as it is shown that thicker walls of a pipe achieve lower amounts of dynamic deflection amplitude. For example, with enhancing the thickness-to-radius of the pipeline from 0.02 to 0.04 and 0.01 to 0.09, the dynamic deflection is reduced from 1.5122 mm to 0.9856 mm and 1.5122 mm to 0.8309 mm, respectively. In another words, increasing the thickness-to-radius of the pipeline from 0.02 to 0.04 and 0.01 to 0.09, the maximum dynamic deflection is decreased about 35% and 52%, respectively. After considering the mechanical behavior, greater thickness to radius ratio causes the increased bending stiffness and axial stiffness of the structure and consequently, the natural festival of the structure and its resistance to seismic excitation. The increased structural stiffness reduces the deformation under equivalent dynamic loading scenario, actually increasing the ability of pipeline to resist vibration and increase the overall seismic performance of pipeline.

The effect of the aspect ratio which is the length-to-radius ratio (*a/R*) on the dynamic deflection

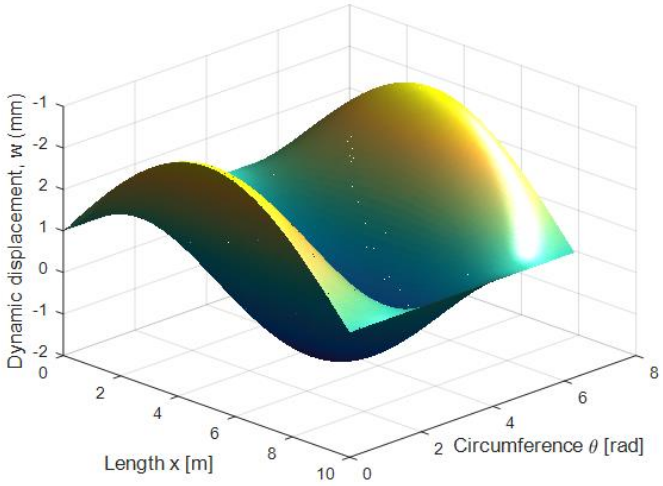

Figure 3. 3D distribution of the dynamic displacement along pipeline length and circumference under internal fluid

of the pipeline over time shown in Table 4. The obtained results show that an increase in aspect ratio leads to an increase in dynamic deflection amplitude. For example, with enhancing the length-to-radius ratio from 5 to 20, the dynamic deflection is increased from 1.0831 mm to 2.8277 mm which shows the increases of 161% in the maximum dynamic deflection. Mechanically, the longer the span compared with the radius of the pipe, the less flexural stiffness and the more slenderness of structure, the more flexible and sensitive to seismic excitation the structure is. This added slenderness reduces natural frequency, but this can invest resonance effects occurring in dynamic loading, an effect which can increase vibration amplitude and deflection.

The spatial distribution of the dynamic displacement along pipeline length and circumference at a typical time instant when the structure is only subjected to internal fluid is plotted in Fig. 3. Its deformation profile is sinusoidal in the axial direction in accordance with the fundamental mode profile of the pipeline and symmetric in the circumferential direction. Its displacement is greatest around the mid-span, where bending stiffness also is weakest, and it is far greater than it is in the empty-pipe instance because the added-mass effect of the internal fluid serves to decrease the structural stiffness. The visualization aids in associating the one dimensional displacement-time plot in the key results and in the deformed structure in the third dimension.

Fig. 4 displays the transient displacement of the pipeline where both internal and external fluid effects were taken into account. The amplitude of displacement is somewhat more prominent than in Fig. 4 throughout the whole structure and the high point of the deflection in the middle of the structure doubles as the trends in the numerical data suggest. The factor behind this amplification is that the outer fluid also decreases the effective stiffness of the system by adding blank loading and fluid structure coupled motions, further increasing the response of the pipeline to the dynamic loads. The shape of the contour variation as a function of the circumference is largely unchanged with respect to the internal-fluid-only case though the overall deformation envelope is more strong to allow a visual interpretation of the synergetic destabilizing effects of both the internal and external fluid under seismic conditions.

The findings of Fig. 5 imply that the higher the content of the SiO_2 nanoparticle the lower the maximum displacement of the pipeline in dynamic fluid load conditions. The structure has the

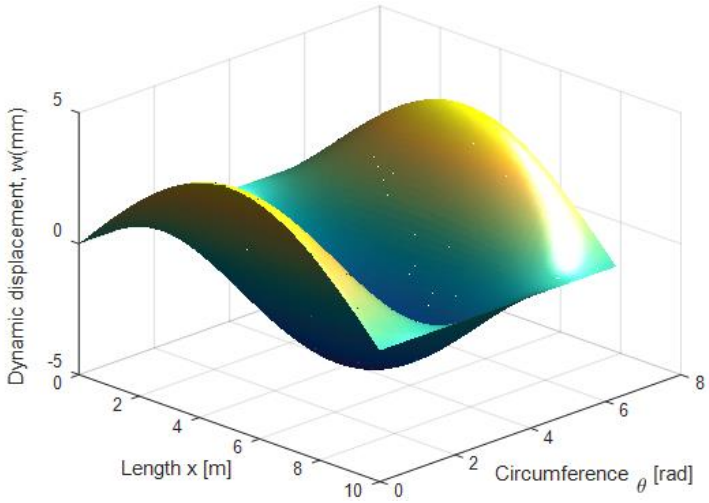

Figure 4. 3D distribution of the dynamic displacement along pipeline length and circumference under internal and external fluids

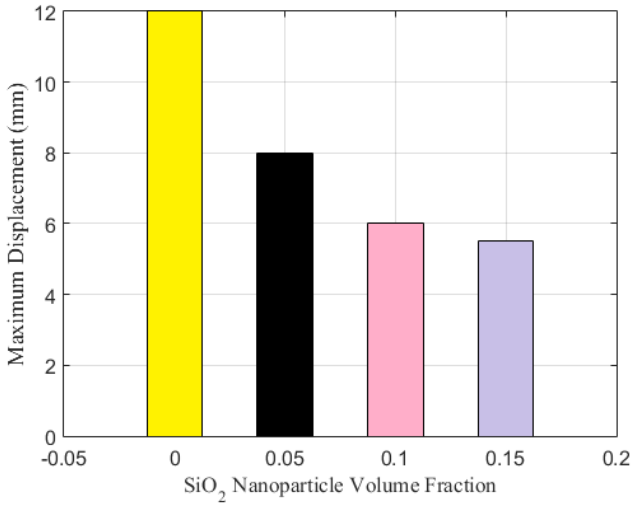

Figure 5. Effect of SiO_2 nanoparticle volume fraction on the maximum deflection

maximum deflection since the stiffness is low and the capacity to resist hydrodynamic forces is less at 0 percent reinforcement. Displacement is reduced significantly by the addition of 0.05 volume fraction and this indicates the positive stiffening influence of nanoparticles. It decreases further at 0.1 volume fraction where the displacement has reduced almost by half as compared to the unreinforced pipe. Nevertheless, the enhancement value levels off with an increase in volume fraction at 0.15 implying diminishing returns due to oversaturation with nanoparticles resulting in clustering and reduced load transfer in the composite matrix. These results indicate the best nanoparticle concentration (0.05- 0.1) to achieve a balance between increasing the stiffness and efficiency of the material in sports water systems pipelines.

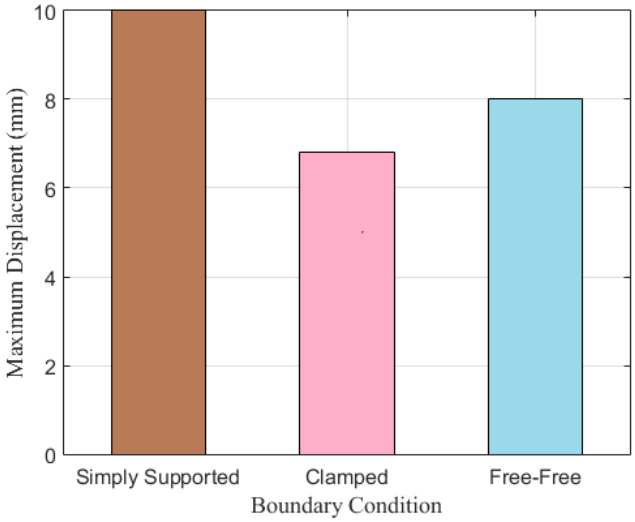

Figure 6. Effect of boundary conditions on the maximum deflection

The structural response of the pipeline in Fig. 6 is greatly influenced by the effects of the boundary conditions. The simply supported system showed the greatest displacement because the system is free to rotate the ends resulting in less resistance to dynamic deformation. Conversely, the level of displacement reduced significantly by up to over 40 percent relative to that in a simply supported case because the constraints associated with fixed ends were more rigidity enforcing. The free-free configuration showed the intermediate behavior which constitutes a lower restraint but higher freedom of structural vibrations. The analysis affirms that structural supports are important in determining hydrodynamic stability of nanocomposite pipelines. In the case of sports hydration systems, it is necessary to consider the support conditions: although clamped supports provide maximum support, a simple supported condition can be practical with a portable system. Thus, trade-offs in engineering have to consider the trade-offs between structural integrity and portability and usability in sporting uses.

5. Conclusions

The present paper explored the hydrodynamic behavior and the dynamic behavior of underwater cylindrical pipelines made up of nanocomposites that carry fluid with the emphasis of its usage in sports water systems to aid in better athletic hydration. Numerical simulations of the effects of the reinforcement of structural behaviour of SiO_2 nanoparticles and fluid structure interaction using the Navier-Stokes equations, classical shell theory, the Hamilton principle and geometric ratios and the internal fluid pressure were systematically studied through numerical simulations. In general, the paper presents important information on how to design lightweight, robust, and energy efficient nanocomposite pipelines in sports hydration systems. With the incorporation of nanomaterials with high-level structural modeling, it will be possible to optimise hydrodynamic performance without sacrificing structural stability under dynamic conditions. These results open the way to the next-generation athletic hydration technologies, which combine

the material innovation, fluid dynamics, and structural engineering to reach the highest level of efficiency and reliability. The structural response was dramatically enhanced with the addition of internal fluid; the minimum deflection is almost five times greater than when the pipeline was empty.

• The lack of outside flow leads to a comparatively lower deflection, whereas the addition of the surrounding fluid leads to a maximum displacement that was increased by about 185%.

• The maximum dynamic deflection of pipe was about 65% lower with respect to augmented ones.

• The simply-simply configuration had the largest deflection (0.9822 mm) compared to clamped-clamped ones (0.4231 mm) which was about 132 % higher.

• Increasing the ratio of thickness to radius from 0.02 to 0.4 caused a decrease of more than 35% in maximum dynamic deflection and the ratio from 0.02 to 0.09 caused a decrease of about 52%.

• Reduction in length-to-radius ratio (5-20) increased the maximum deflection by 161%.

• When nanoparticle volume fraction was raised from 0 (pipe without nanoparticles) up to 0.1 superficially, the maximum deflection was reduced by 71%.

The current examination is based on seismic response of the pipeline considering nanocomposites along with the internal and external fluid. There was no consideration of non-seismic loads, multiphase fluid effects, thermal or operational loads and other combinations of loading. Responses may therefore differ outside these parameters or in real conditions of building and manufacturing flaws, corrosion or complicated loading. However, these topics will be studied in future works.

References

1. Benjamin, T.B. (1961). Dynamics of a system of articulated pipes conveying fluid. Proceedings of the Royal Society of London. Series A, 261(130), 457-486. https://doi.org/10.1098/rspa.1961.0090.
2. Amabili, M., Pellicano, F., Païdoussis, M.P. (1999). Non-linear dynamics and stability of circular cylindrical shells containing flowing fluid. Part II: Large-amplitude vibrations without flow. Journal of Sound and Vibration, 228, 1103-1124. https://doi.org/10.1006/jsvi.1999.2476.
3. Yoon, H.I., Son, I. (2007). Dynamic response of rotating flexible cantilever pipe conveying fluid with tip mass. International Journal of Mechanical Sciences, 49, 878-887. https://doi.org/10.1016/j.ijmecsci.2006.11.006.
4. Amabili, M. (2008). Nonlinear Vibrations and Stability of Shells and Plates. Cambridge University Press, Cambridge.
5. Alijani, F., Amabili, M. (2014). Nonlinear vibrations and multiple resonances of fluid-filled arbitrary laminated circular cylindrical shells. Composite Structures, 108, 951-962. https://doi.org/10.1016/j.compstruct.2013.10.029.
6. Thinh, T.I., Nguyen, M.C. (2016). Dynamic stiffness method for free vibration of composite cylindrical shells containing fluid. Applied Mathematical Modelling, 40, 9286-9301. https://doi.org/10.1016/j.apm.2016.06.015.
7. Zhou, X.Q., Yu, D.Y., Shao, X.Y., Zhang, C.Y., Wang, S. (2017). Dynamics characteristic of steady fluid conveying in the periodical partially viscoelastic composite pipeline. Composites Part B: Engineering, 111, 387-408. https://doi.org/10.1016/j.compositesb.2016.11.059.
8. Wu, J.H., Sun, Y.D., Su, M.Z., Hao, X.Y., He, T. (2022). Band gap analysis of composite fluid-filled pipe with periodically axial support or dynamic vibration absorbers. Mechanics of Advanced Materials and Structures, 30(20), 4082-4090. https://doi.org/10.1080/15376494.2022.2088908.

9. Oke, W.A., Khulief, Y.A., Owolabi, T.O., Ikumapayi, O.M (2024). Dynamic analysis of a multi-span pipe conveying fluid using wavelet based finite element method. Arabian Journal for Science and Engineering, 49, 14663-14682. https://doi.org/10.1007/s13369-024-08753-9.
10. Hu, J., Ma, D., Cao, R., Chen, W., Dai, H., Wang, L. (2025). Buckling and dynamical behaviors of hard magnetic soft pipe conveying fluid under distributed spring constraint. Acta Mechanica Solida Sinica. https://doi.org/10.1007/s10338-025-00619-3.
11. Su, J., Yao, G. (2025). Influence of cracks on the nonlinear dynamic behaviors of pipes conveying fluid. Mechanics Based Design of Structures and Machines, 1-22. https://doi.org/10.1080/15397734.2025.2491798.
12. Wang, Y., Xu, F.. Guo, C. (2025). Stability of fluid-conveying pipe in mining transportation system with elastic supports under distributed follower force. Mechanics of Solids, 60, 737-748. https://doi.org/10.1134/S0025654424607092.
13. Youn, H., Je Oh, H., Kim, D. (2021). Prioritizing water distribution pipe renewal based on seismic risk and construction cost. Membranes and Water Treatment, 12, 195-204. https://doi.org/10.12989/mwt.2021.12.5.195.
14. Zamani Nouri, A. (2017). Mathematical modeling of concrete pipes reinforced with CNTs conveying fluid for vibration and stability analyses. Computers and Concrete, 19(3), 325-331. https://doi.org/10.12989/cac.2017.19.3.325.
15. Meng, Y., Xu, Z. and Zamani Nouri, A. (2025). Nanoparticle influence on the behavior of membrane-based water treatment for enhancing hydration quality in athletic structures: A comprehensive analysis. Membranes and Water Treatment, 16, 249-257. https://doi.org/10.12989/mwt.2025.16.5.249.
16. Sun, L., Zamani Nouri, A. and Yvaz, A. (2024). Water force and the dynamics of pipes through innovative perspectives on flow and structure in fine art. Membranes and Water Treatment, 15, 177-183. https://doi.org/10.12989/mwt.2024.15.4.177.
17. Yuan, G., Song, J., Yang, Y., Ni, B., Yang, D., Xue, Y. (2025). Experimental study on icebreaking mechanism and failure modes of submerged high-pressure water jets. Ocean Engineering, 323, 120586. https://doi.org/10.1016/j.oceaneng.2025.120586.
18. Yuan, G., Wang, X., Ni, B., Xu, W., Yang, D., Xue, Y. (2025). Experimental study on load characteristic and icebreaking process of submerged Venturi cavitating water jets. Journal of Fluids and Structures, 137, 104374. https://doi.org/10.1016/j.jfluidstructs.2025.104374.
19. Liu, X., Cai, X., Huang, Z., Hou, Y., Qin, J., Chen, Z. (2025). Comparative study on the oblique water-entry of high-speed projectile based on rigid-body and elastic-plastic body model. Defence Technology, 46, 133-155. https://doi.org/10.1016/j.dt.2024.11.007.
20. Zhang, H., Li, K., Liu, T., Liu, Y., Hu, J., Zuo, Q., Jiang, L. (2025). Analysis of Radial Hydraulic Forces in Centrifugal Pump Operation via Hierarchical Clustering (HC) Algorithms. Applied Sciences, 15(18), 10251. https://doi.org/10.3390/app151810251.
21. Li, L.N., Chen, J.H., Gao, C.Ø., Zhou, Z.H., Li, M., Zhang, D., Chen, X.H. (2025). Peridynamics simulation of hydraulic fracturing in three-dimensional fractured rock mass. Physics of Fluids, 37(7), 73628. https://doi.org/10.1063/5.0274871.
22. Ren, K., Miao, J., Qing, H., Xu, W., Zhang, X., He, Z., Lu, F. (2025). Probing to dynamics of a tube-core sandwich enhanced liquid-filled tank subjected to hydrodynamic ram. Thin-Walled Structures, 215, 113573. https://doi.org/10.1016/j.tws.2025.113573.
23. Yuan, G., Ni, B., Kim, D.K. (2025). Ice fracture behaviours in cavitating waterjet-ice interaction with initial defects in ice. Ocean Engineering, 342, 122870. https://doi.org/10.1016/j.oceaneng.2025.122870
24. Hao, G., Yu, R., Dong, X., Li, Z. (2026). Simulation of droplet impacting on elastic pillars using smoothed particle hydrodynamics method. Journal of Fluids and Structures, 143, 104541. https://doi.org/10.1016/j.jfluidstructs.2026.104541
25. Huang, B. Q., & Li, X. (2023). Wave Attenuation by Sea Ice in the Arctic Marginal Ice Zone Observed by Spaceborne SAR. Geophysical Research Letters, 50(21), e2023GL105059. doi: https://doi.org/10.1029/2023GL105059
26. Chen, D., Zhang, W., Li, C., Ma, L., Shi, X., Li, H., Zhu, H. (2025). Randomly generating realistic

calcareous sand for directional seepage simulation using deep convolutional generative adversarial networks. Journal of Rock Mechanics and Geotechnical Engineering. https://doi.org/10.1016/j.jrmge.2025.01.055

27. Yi, Z., Qiu, C., Wang, D., Cai, Z., Yu, J., Shi, J. (2024). Submesoscale Kinetic Energy Induced by Vertical Buoyancy Fluxes During the Tropical Cyclone Haitang. Journal of Geophysical Research: Oceans, 129(7), e2023JC020494. https://doi.org/10.1029/2023JC020494
28. Zhao, G., Gao, H., Qu, Z., Fan, H., Meng, H. (2023). Anhydrous interfacial polymerization of sub-1 Å sieving polyamide membrane. Nature Communications, 14(1), 7624. https://doi.org/10.1038/s41467-023-43291-2
29. Yuan, G., Ni, B., Liu, P., Kim, D.K. (2025). Ice damage characteristics under high-pressure water jet based on JohnsonHolmquist II brittle constitutive model. Physics of Fluids, 37(8), 86153. https://doi.org/10.1063/5.0282983
30. Yuan, L., He, W., Wu, X., Kong, Y., Yang, Y., Ramsey, T.S., ... Degefu, D.M. (2026). Allocating water resources in transboundary river basins: A sequential rubinstein bargaining approach with risk discounting. Journal of Hydrology: Regional Studies, 63, 102989. https://doi.org/10.1016/j.ejrh.2025.102989
31. Gao, J., Luo, J., Yin, S., Gong, C., Wang, S., Zhang, G. (2026). Adaptive Digital Twin Framework for PMSM Thermal Safety Monitoring: Integrating Bayesian Self-Calibration with Hierarchical Physics-Aware Network. Machines, 14(2), 138. https://doi.org/10.3390/machines14020138
32. Dai, H., Yang, Y., Zhang, F., Guadagnini, A., Yang, J., Bu, X., ... Ye, M. (2026). Identification of Key Factors Driving Dissolved Oxygen in Riparian Aquifers Through Deep Learning-Assisted Global Sensitivity Analysis. Water Resources Research, 62(2), e2025WR041884. https://doi.org/10.1029/2025WR041884
33. Li, J., Liu, Q., Liang, B., Sun, W., Jin, J., Liu, J., ... Li, C. (2026). Mechanical properties of sandstones damaged by co2 reactions and flow characteristics under complex mixed-wettability. Energy & Fuels, 40(4), 2108-2125. https://doi.org/10.1021/acs.energyfuels.5c05804
34. Zhou, Y., Zhang, Y., Zhussupbekov, A., Zhang, C., Guan, W. (2026). Pore-scale study of drainage behavior in gradient porous media. Physics of Fluids, 38(2). https://doi.org/10.1063/5.0313379
35. Cheng, L., Lu, H., Guo, B., Liang, Q., Han, P., Li, Z., ... Du, P. (2026). Fast prediction of underwater vehicle motion under internal solitary waves. Physics of Fluids, 38(2), 27115. https://doi.org/10.1063/5.0315969
36. Dai, Z., Wang, C., Peng, R., Jiang, M. (2026). Evaluating the impact force of submarine landslide on pipelines: insights from flume tests and multiphase flow model analysis. Ocean Engineering, 352, 124629. https://doi.org/10.1016/j.oceaneng.2026.124629
37. Zhu, C., Tao, S., Zhu, Q., Wu, C., Gao, A., ... Mei, S. (2026). Different roles of submerged aquatic vegetations in open-channel flow and wind-induced flow. Physics of Fluids, 38(2), 21915. https://doi.org/10.1063/5.0311462